NATIONAL ADVISORY COMMITTEE FOR AERONAUTICS

TECHNICAL NOTE 2923

STUDY OF MOTION OF MODEL OF PERSONAL-OWNER OR LIAISON AIRPLANE THROUGH THE STALL AND INTO THE INCIPIENT SPIN BY MEANS OF A FREE-FLIGHT TESTING TECHNIQUE

By Ralph W. Stone, Jr., William G. Garner, and Lawrence J. Gale

Langley Aeronautical Laboratory
Langley Field, Va.

Washington
April 1953

1E

NATIONAL ADVISORY COMMITTEE FOR AERONAUTICS

TECHNICAL NOTE 2923

STUDY OF MOTION OF MODEL OF PERSONAL-OWNER OR LIAISON AIRPLANE THROUGH THE STALL AND INTO THE INCIPIENT SPIN BY MEANS OF A FREE-FLIGHT TESTING TECHNIQUE

By Ralph W. Stone, Jr., William G. Garner, and Lawrence J. Gale

SUMMARY

A study of the motion of a personal-owner or liaison airplane through the stall and into the incipient spin has been made by catapulting a dynamic model into still air. The results showed that the model became unstalled in inverted flight after its initial rotation of substantially 180° in roll. Since the rates of rotation were low, it may be inferred that termination of the incipient spin would be most readily obtained by proper control movements at this point.

INTRODUCTION

Statistics indicate that a large percentage of all fatal private flying accidents in the past have occurred because of pilot error; in more than half of these accidents, the airplane stall has been involved (ref. 1). Oftentimes, accidents of this nature are referred to as "stall-spin" accidents and they occur primarily in the incipient phase of a spin, that is, in that portion of the motion immediately following the stall and before a spin can fully develop. In addition, spin demonstrations of some airplanes for the armed services require recoveries from only two-turn spins which also may not be fully developed motions. Data on the incipient spin are not available although much effort has been expended in the Langley 20-foot free-spinning tunnel toward an understanding of the developed spin. The problems associated with the incipient phase of the spin may be quite different from those associated with the fully developed spin and recovery therefrom.

A technique is being developed with free dynamic models, similar to those used in spin testing, to study the incipient spin. The model is catapulted into still air in such a manner that stalled flight occurs,

and the ensuing motion at and beyond the stall is studied by use of motion-picture records from which the angles of attack and sideslip and the linear and angular velocities are determined. Scale effect could greatly influence the motion at and just beyond the stall although it has been shown to be of only secondary importance in developed spins. The technique described, therefore, may be used primarily to isolate the effects of various parameters rather than to indicate specific incipient-spin characteristics. The initial investigation was performed to determine the motion in the incipient spin of a model of a low-wing, single-vertical-tail airplane typical of a present-day four-place personal-owner or liaison airplane and to determine the extent to which the motion may repeat itself. The results of this investigation are reported herein.

SYMBOLS

The analysis of the motion was made with respect to the body system of axes. A diagram of these axes showing various angles pertinent to the analysis is given in figure 1.

X,Y,Z	earth axes, a system of mutually perpendicular axes through airplane center of gravity always perpendicular and parallel to earth's surface and of constant direction
X_B,Y_B,Z_B	body axes
$x_{r_R},x_{r_T},x_{r_{cg}}$	distance along X earth axis from reference point to right wing tip, tail, and center of gravity, respectively
$y_{r_R},y_{r_T},y_{r_{cg}}$	distance along Y earth axis from reference point to right wing tip, tail, and center of gravity, respectively
$z_{r_R},z_{r_T},z_{r_{cg}}$	distance along Z earth axis from reference point to right wing tip, tail, and center of gravity, respectively
x_R,y_R,z_R	distance of right wing tip from center of gravity along X, Y, and Z earth axes, respectively
x_T,y_T,z_T	distance of tail from center of gravity along X, Y, and Z earth axes, respectively
b	span of model, ft
l_T	tail length (distance between center of gravity and intersection of X_B with trailing edge of rudder), ft

$\bar{c}$	mean aerodynamic chord, ft
$x/\bar{c}$	ratio of distance of center of gravity rearward of leading edge of mean aerodynamic chord to mean aerodynamic chord
$z/\bar{c}$	ratio of distance between center of gravity and fuselage reference line to mean aerodynamic chord (positive when center of gravity is below fuselage reference line)
m	mass of airplane, slugs
$I_{X_B}, I_{Y_B}, I_{Z_B}$	moments of inertia about X_B, Y_B, and Z_B axes, respectively, slug-feet^2
$\frac{I_{X_B} - I_{Y_B}}{mb^2}$	inertia yawing-moment parameter
$\frac{I_{Y_B} - I_{Z_B}}{mb^2}$	inertia rolling-moment parameter
$\frac{I_{Z_B} - I_{X_B}}{mb^2}$	inertia pitching-moment parameter
ρ	air density, slugs/cu ft
V	resultant velocity of center of gravity, ft/sec
u,v,w	components of velocity V along X, Y, and Z earth axes, respectively, ft/sec
u_B, v_B, w_B	components of velocity V along X_B, Y_B, and Z_B axes, respectively, ft/sec
α	angle of attack, $\tan^{-1}\frac{w_B}{u_B}$, deg
β	angle of sideslip, $\sin^{-1}\frac{v_B}{V}$, deg
h	altitude loss, ft
p	rolling angular velocity about X_B, radians/sec

q	pitching angular velocity about Y_B, radians/sec
r	yawing angular velocity about Z_B, radians/sec
OA and OC	projections of X_B and Y_B, respectively, on earth X,Y plane (fig. 1)
OB	position X_B would take if airplane were rotated about Y_B until X_B lay in earth X,Y plane (fig. 1)
OD	position Y_B would take if airplane were rotated about X_B until Y_B lay in earth X,Y plane (fig. 1)
OE	position Z_B would take if airplane were rotated about Y_B until X_B lay in earth X,Y plane (fig. 1)
OF	position Z_B would take if airplane were rotated about X_B until Y_B lay in earth X,Y plane (fig. 1)
θ	angle that X_B axis makes with earth X,Y plane, positive when nose is above plane (Euler's angle θ)
ϕ	angle between Y_B and line OD (fig. 1) (Euler's angle ϕ)
ψ	angle between X earth axis and OA measured as shown in figure 1 from 0° to 360° (Euler's angle ψ)
$\dot{\psi}$	rate of change of ψ with time, radians/sec
$\dot{\phi}$	rate of change of ϕ with time, radians/sec
$\dot{\theta}$	rate of change of θ with time, radians/sec
ψ'	angle between Y earth axis and OC measured as shown in figure 1 from 0° to 360°
ϕ'	angle that Y_B axis makes with earth X,Y plane positive when right wing is below plane
θ'	angle between X_B and line OB (fig. 1)
ψ''	angle in X,Y plane between OA and OB or between OC and OD (fig. 1)

APPARATUS AND METHODS

Model

The model used in this investigation was a configuration similar with respect to mass and dimensional characteristics to one investigated in reference 2 for fully developed spin and recovery characteristics. Based on the model size and the average dimensions obtained for a large number of personal-owner airplane designs, the model may be considered to be a 1/12.4 scale of a personal-owner or liaison airplane. The weight and moments of inertia of the model represent those of an airplane typical of this type. A three-view drawing of the model is shown in figure 2 and the mass and dimensional characteristics of a corresponding full-scale airplane are tabulated in table I.

The model was constructed principally of balsa and reinforced with spruce and cedar. A photograph of the model is shown in figure 3. In accordance with spin-tunnel practice, the propeller and landing gear were not simulated on the model. The model wing had an NACA 43012 airfoil section which at low Reynolds number has a sharp break in the lift curve at the stall. (See ref. 3.)

Apparatus

The tests were performed inside a building approximately 70 feet square and 60 feet high. The launching apparatus, shown in figure 4, was located 55 feet above the floor near one wall of the building and consisted primarily of an elastic chord which catapulted the model from its launching platform along a short track. The launching platform could be adjusted to set the model attitude and thus the launching angle of attack. An electronic timer was used to measure the model velocity just after it was launched. Fixed motion-picture cameras were located along the walls parallel and perpendicular to the initial launching direction to record the model motion. The cameras had overlapping fields so that the model was in view of at least two of the cameras, located at right angles to one another, throughout its flight. The motion-picture records were synchronized by use of a common timing light reflected into the camera fields. A large net for model retrieving purposes was hung from the wall opposite the launching apparatus.

Testing Technique

The model was catapulted from the launching apparatus at a speed slightly in excess of the stalling speed and at an angle of attack just

below the stall angle of attack. The elevator control of the model was set so as to pitch the model from the launching angle of attack up through the stall and the rudder was set to initiate a yawing motion and thus to precipitate a roll-off after stalling.

As previously mentioned, photographic time histories of the model motion were made with a system of motion-picture cameras arranged so as to have the model in the field of two cameras with perpendicular focal axes at all times. When at an instant of time the model is in the field of two cameras located at right angles to one another, the space coordinates of the model can be determined. By this means, the model could be located at any instant from the time of catapult until the time the model struck the retrieving net. From a knowledge of the space coordinates and their instantaneous time values, the velocities of the model were obtained along the earth axes. Then, the attitude of the model at any instant being known, angle of attack, angle of sideslip, and linear and angular velocities were calculated. The derivation of equations for these calculations is presented in the appendix.

Test Conditions and Accuracy

For the tests, the model was ballasted with lead weights to represent a corresponding airplane at an altitude of 5,000 feet (ρ = 0.002049 slug/cu ft).

For this investigation, the controls of the model were set so as to cause the model to stall and enter a spin soon after launching. The settings of the controls were as follows:

Elevator full up, deg	30
Ailerons, deg	0
Rudder fully deflected (in direction desired for roll-off), deg	30

The stalling angle and stalling speed of the model were determined from force tests of the model conducted on a strain-gage balance in the Langley 20-foot free-spinning tunnel. The Reynolds number of the present investigation was approximately 1×10^5 based on the mean aerodynamic chord of the model.

Errors in the measured motion were magnified because graphical differentiation was required in reducing the data. For the current tests, the accuracy was estimated to be within the following limits:

α, deg	±5
β, deg	±4
u, v, w (full scale), ft/sec	±1.3
u_B, v_B, w_B(full scale), ft/sec	±4.9
p, q, r (full scale), radians/sec	±0.15
Altitude loss (full scale), ft	±1
Weight, percent	±1
Center-of-gravity position, percent $\bar{c}$	±1
Moments of inertia, percent	±5
Control settings, deg	±1

RESULTS AND DISCUSSION

The results of the tests are presented in figures 5 and 6. The model test data have been converted to full-scale values for a corresponding airplane at a test altitude of 5,000 feet based on the premise that the model scale was 1/12.4. Film strips showing the motion of the model as it stalls and enters a spin are presented in figure 7.

The results as the model rolled to the right and entered an incipient spin are presented in figure 5 for an initial and a repeat test. Variations with time of the angle of attack, angle of sideslip, altitude loss, and the rates of roll, pitch, and yaw are given in figure 5. Sketches of the approximate attitude of the model at various phases of the motion are also shown in figure 5. As was previously noted, the elevator was full up (30°) and the rudder was full right (30°) for these tests. Soon after the model stalled, it again became unstalled (time, approx. 1.75 sec), went inverted for a part of its motion, and assumed a very low angle of attack momentarily before again stalling and continuing toward a developed spin motion, such as reported in reference 2. After the initial stall and immediately after the model became unstalled, the rates of yaw and pitch were relatively small and the rate of roll began to decrease. There also was little loss of altitude up to this time and the results indicated that, even though the airplane may be inverted, a time soon after the roll-off has started appears to be a desirable time to attempt to terminate the motion. This conclusion is in agreement with pilots' experience that recoveries attempted soon after an airplane stalls and rolls off are more readily obtainable than those attempted from developed spins.

The motion obtained may be qualitatively analyzed as follows: After being launched, the model immediately pitched up and yawed right because of the initial settings of the elevator and rudder, respectively. As the motion progressed, the sideslip angle β became negative because of the yawing motion; this sideslip angle tended to cause the model to roll off as a result of the dihedral effect. As was previously noted, the wing

had an NACA 43012 airfoil section for which the lift curve has a sharp break at the stall (ref. 3); this effect undoubtedly augmented the model roll-off because of a loss in damping in roll beyond the stall. When the model again became unstalled, the damping in roll led to decreased rate of roll (p) until the stall reoccurred with the resulting increase in rate of roll. Changes in sideslip angle occurred as the model rolled and increments of positive and negative velocity components along the Y_B axis were obtained as the right or left wing, respectively, was inclined downward.

One of the main objectives of the investigation was to ascertain whether motions through the stall and into the incipient spin could be reliably indicated by means of free dynamic models. The repeat test, the results of which are shown in figure 5, was made with the test conditions nearly the same, insofar as the available equipment allowed, as those of the original or initial test in order to determine whether the motion would repeat itself. Although there were some differences for the repeat test in that the model had a more positive pitching velocity and a somewhat different sideslip angle than for the initial test, the results in general are in good agreement. Quantitatively, the results are generally close to or within the estimated limits of accuracy and indicate that the model probably repeats its motions for similar launching conditions. Because of the unsteady nature of the air flow which exists at and beyond the stall, it has been thought that airplanes may not repeat motions in the stalled-flight regime. The results from the repeat test and experience in spin and spin-recovery work, however, indicate that motions at and beyond the stall may generally repeat themselves except for critical cases such as have been encountered in studies of developed spins when the spin and recovery change unaccountably.

The motions discussed are for power-off stalls and the use of power may appreciably alter the motion or the symmetry from that presented herein. The results should not be interpreted as representing the motions of an airplane corresponding precisely to the model, because of scale effects, but can be considered indicative of the trends in the motion of a typical personal-owner or liaison airplane. Changes in configuration, wing loading, and mass distribution also may alter the results appreciably.

In order to evaluate the symmetry of the model and to ascertain that the motion to the right previously discussed was not influenced primarily by model asymmetry, tests were conducted to determine the motion with the rudder set full left (30°). The results are presented in figure 6. As before, the variation of angle of attack, angle of sideslip, and angular velocities with time are presented as the model stalled and rolled to the left prior to entering a spin to the left.

A comparison of figure 6 with figure 5 indicates that the model, which appeared to be dimensionally symmetrical, showed generally similar motions when the rudder was set either to the right or to the left.

CONCLUDING REMARKS

An investigation has been conducted to study the motion of a free dynamic model of a personal-owner or liaison airplane through the stall and into the incipient spin. This dynamic-model technique does not lend itself to specific or development studies of a given design because of probable scale effects existing at the stall; however, the method is applicable for indicating the trends of the motion through the stall and into the incipient spin and possibly the effect of certain parameters on this motion. The results showed that the model became unstalled in inverted flight after its initial rotation of substantially 180° in roll. Since the rates of rotation were low, it may be inferred that termination of the incipient spin would be most readily obtained by proper control movements at this point. The results of the model flights show that the motion is generally repeatable and that, power effects being excluded, a geometrically symmetrical model should have fairly symmetrical motions to the right and to the left.

Langley Aeronautical Laboratory,
National Advisory Committee for Aeronautics,
Langley Field, Va., January 28, 1953.

APPENDIX

DERIVATION OF EQUATIONS FOR EVALUATION OF PARAMETERS IN INCIPIENT-SPIN MOTION

The determination of angle of attack, angle of sideslip, and the angular velocities of the model in flight are based upon calculating its component velocities along the body axes. The determination of these velocities is accomplished by differentiating the respective earth-axis space coordinates of the model against time to obtain the earth-axes velocities of the model and then resolving by trigonometric means these velocities to a body-axes system. The following process was used.

If X, Y, and Z are the earth axes, and X_B, Y_B, and Z_B are the body axes, both systems having their origin at the center of gravity of the model, the relationships between earth-axes velocities and body-axes velocities are as follows:

$$u_B = u \cos \angle XX_B + v \cos \angle YX_B + w \cos \angle ZX_B \tag{A1}$$

$$v_B = u \cos \angle XY_B + v \cos \angle YY_B + w \cos \angle ZY_B \tag{A2}$$

$$w_B = u \cos \angle XZ_B + v \cos \angle YZ_B + w \cos \angle ZZ_B \tag{A3}$$

where $\angle XX_B$, $\angle YX_B$, and so forth, are angles between the earth and body axes designated. These nine angles, which relate the velocities along the earth and body axes through direction cosines, therefore must be found. The coordinates of the model right wing and tail reference points

(wing tip in X_B,Y_B plane and tail cone in X_B,Z_B plane, respectively) from the center of gravity are determined:

$$x_R = x_{r_R} - x_{r_{cg}}$$

$$y_R = y_{r_R} - y_{r_{cg}}$$

$$z_R = z_{r_R} - z_{r_{cg}}$$

$$x_T = x_{r_T} - x_{r_{cg}}$$

$$y_T = y_{r_T} - y_{r_{cg}}$$

$$z_T = z_{r_T} - z_{r_{cg}}$$

From the foregoing coordinates, the angles θ, ψ, ϕ', ψ', θ', and ϕ, as well as ψ'', can be obtained (see fig. 1):

$$\left.\begin{aligned}
\theta &= \sin^{-1}\frac{z_T}{l_T} \\
\psi &= \tan^{-1}\frac{y_T}{x_T} \\
\phi' &= \sin^{-1}\frac{z_R}{b/2} \\
\psi' &= \tan^{-1}\frac{-x_R}{y_R} \\
\psi'' &= \psi' - \psi \\
\theta' &= \cos^{-1}(\cos\theta\cos\psi'') \\
\phi &= \cos^{-1}(\cos\phi'\cos\psi'')
\end{aligned}\right\} \qquad (A4)$$

From figures 1 and 8 and from the determination of the angles calculated in equations (A4), the trigonometric functions necessary for the solution of equations (A1) and (A2) can be obtained as follows:

$$\cos \angle XX_B = \cos \psi \cos \theta \tag{A5}$$

$$\cos \angle YX_B = \cos(90 - \psi)\cos \theta = \sin \psi \cos \theta \tag{A6}$$

$$\cos \angle ZX_B = \cos(90 + \theta) = -\sin \theta \tag{A7}$$

$$\cos \angle YY_B = \cos \psi' \cos \phi' \tag{A8}$$

$$\cos \angle XY_B = \cos(90 + \psi')\cos \phi' = -\sin \psi' \cos \phi' \tag{A9}$$

$$\cos \angle ZY_B = \cos(90 - \phi') = \sin \phi' \tag{A10}$$

The determination of the trigonometric functions needed for the solution of equation (A3) is somewhat more difficult than those for equations (A1) and (A2). These functions may be found by consideration of the spherical triangles depicted in figure 8.

$$\cos \angle ZZ_B = \cos \theta \cos \phi = \cos \theta' \cos \phi' \tag{A11}$$

Also, from figure 8

$$\cos \angle XZ_B = \sin \angle ZZ_B \cos \angle XZZ_B$$

where

$$\sin \angle ZZ_B = \sqrt{1 - \cos^2\theta \cos^2\phi}$$

and

$$\cos \angle XZZ_B = \cos \psi \cos \angle Z_BZF + \sin \psi \sin \angle Z_BZF$$

or

$$\cos \angle XZZ_B = \frac{\cos \psi \sin \theta \cos \phi + \sin \psi \sin \phi}{\sqrt{1 - \cos^2\theta \cos^2\phi}}$$

Therefore,

$$\cos \angle XZ_B = \cos \psi \sin \theta \cos \phi + \sin \psi \sin \phi \qquad \text{(A12)}$$

Now

$$\cos \angle YZ_B = \sin \angle ZZ_B \cos \angle YZZ_B$$

where

$$\cos \angle YZZ_B = \sin \psi \cos \angle Z_BZF - \cos \psi \sin \angle Z_BZF$$

or

$$\cos \angle YZZ_B = \frac{\sin \psi \sin \theta \cos \phi - \cos \psi \sin \phi}{\sqrt{1 - \cos^2\theta \cos^2\phi}}$$

Therefore,

$$\cos \angle YZ_B = \sin \psi \sin \theta \cos \phi - \cos \psi \sin \phi \qquad (A13)$$

(Note that angles XZZ_B, YZZ_B, and Z_BZF are angles between the arcs of the spherical triangles shown in figure 8.) Thus, with the equations (A5) to (A13), the nine necessary direction cosines are determined and equations (A1) to (A3) may be solved for the velocities along the body axes. The velocities along the earth axes necessary for the solution of these equations are obtained, as was indicated previously, by taking the first derivative of the space coordinates with respect to time.

From a solution of equations (A1) and (A3) wherein a determination of the velocities of the center of gravity along the X and Z body axes has been made, the angle of attack, measured at the center of gravity and defined as the angle between the X body axis and the projection of the relative wind on the X_B,Z_B plane, can be calculated as follows:

$$\alpha = \tan^{-1} \frac{w_B}{u_B} \qquad (A14)$$

If the resultant velocity of the model is calculated

$$V = \sqrt{u_B^2 + v_B^2 + w_B^2} \qquad (A15)$$

the angle of sideslip may be calculated as follows:

$$\beta = \sin^{-1} \frac{v_B}{V} \qquad (A16)$$

For a determination of the angular velocities p, q, and r, reference 4 was used. The angular velocities are determined on the basis of

Euler's angles, which are herein defined as ψ, θ, and ϕ. The equations for the angular velocities therefore are as follows:

$$p = \dot{\phi} - \dot{\psi} \sin \theta \tag{A17}$$

$$q = \dot{\theta} \cos \phi + \dot{\psi} \sin \phi \cos \theta \tag{A18}$$

$$r = \dot{\psi} \cos \phi \cos \theta - \dot{\theta} \sin \phi \tag{A19}$$

REFERENCES

1. Lankford, Jesse W.: Accident Statistics Can Contribute to Safer Flying. Mech. Eng., vol. 72, no. 7, July 1950, pp. 553-555, 558.

2. Klinar, Walter J., and Wilson, Jack H.: Spin-Tunnel Investigation of the Effects of Mass and Dimensional Variations on the Spinning Characteristics of a Low-Wing Single-Vertical-Tail Model Typical of Personal-Owner Airplanes. NACA TN 2352, 1951.

3. Jacobs, Eastman N., and Sherman, Albert: Airfoil Section Characteristics As Affected by Variations of the Reynolds Number. NACA Rep. 586, 1937.

4. MacMillan, William Duncan: Theoretical Mechanics. Dynamics of Rigid Bodies. First ed., McGraw-Hill Book Co., Inc., 1936, p. 185.

TABLE I.- DIMENSIONAL AND MASS CHARACTERISTICS OF THE CORRESPONDING FULL-SCALE AIRPLANE

Dimensional:	
Over-all length, ft	22.37
Wing:	
Airfoil section	NACA 43012
Incidence, deg	3
Dihedral, deg	6
Twist, deg	0
Span, ft	33.63
Mean aerodynamic chord, $\bar{c}$, ft	4.89
Leading edge of mean aerodynamic chord rearward of leading edge of wing, ft	0.05
Taper ratio	1.00
Area, sq ft	163.28
Aspect ratio	6.93
Ailerons:	
Span, ft	7.15
Area, rearward of hinge line, sq ft	15.70
Horizontal-tail surface:	
Span, ft	10.25
Total area, sq ft	26.39
Elevator area rearward of hinge line, sq ft	11.02
Aspect ratio	3.98
Incidence, deg	0
Dihedral, deg	0
Distance from quarter chord of $\bar{c}$ to elevator hinge line, ft	13.73
Section	Modified NACA 0009
Vertical-tail surface:	
Span, ft	5.32
Total area, sq ft	12.96
Rudder area rearward of hinge line, sq ft	6.48
Aspect ratio	1.26
Offset, deg	0
Distance from quarter chord $\bar{c}$ to rudder hinge line, ft	14.18
Section	Modified NACA 0009
Mass:	
Weight, lb	2449
Wing loading, lb/sq ft	15.0
Relative density:	
Sea level	5.82
5,000 ft	6.76
Center of gravity:	
$x/\bar{c}$	0.26
$z/\bar{c}$	0.12
Moments of inertia (about center of gravity), slug-ft^2	
I_{X_B}	2387
I_{Y_B}	1998
I_{Z_B}	4186
Inertia parameters:	
$\frac{I_{X_B} - I_{Y_B}}{mb^2}$	45
$\frac{I_{Y_B} - I_{Z_B}}{mb^2}$	-251
$\frac{I_{Z_B} - I_{X_B}}{mb^2}$	206

NACA

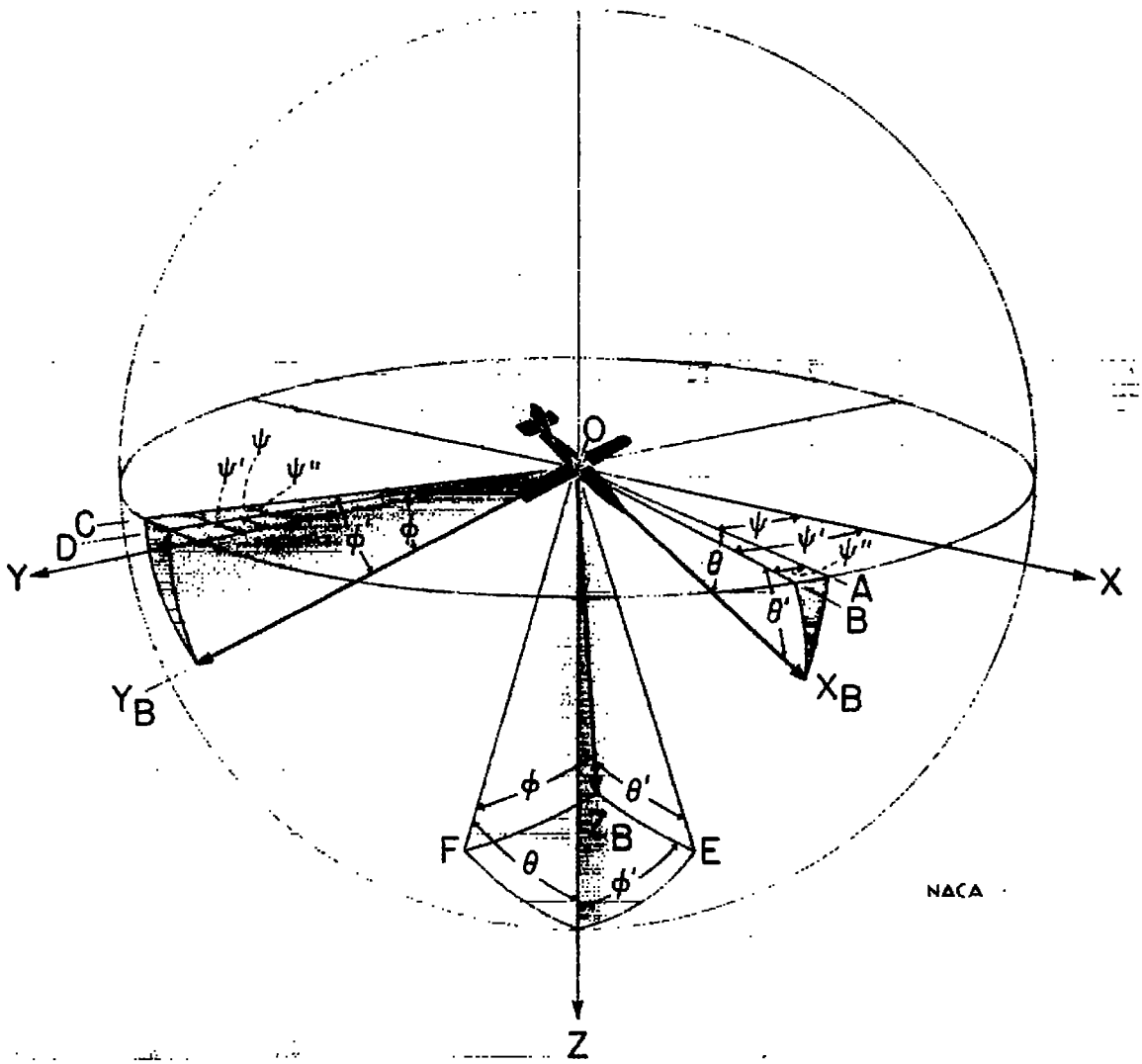

Figure 1.- Diagram of earth and body axes through the center of gravity of the model showing angular relations. Positive directions of axes and positive values of angles are shown except for θ and θ' which are shown negative.

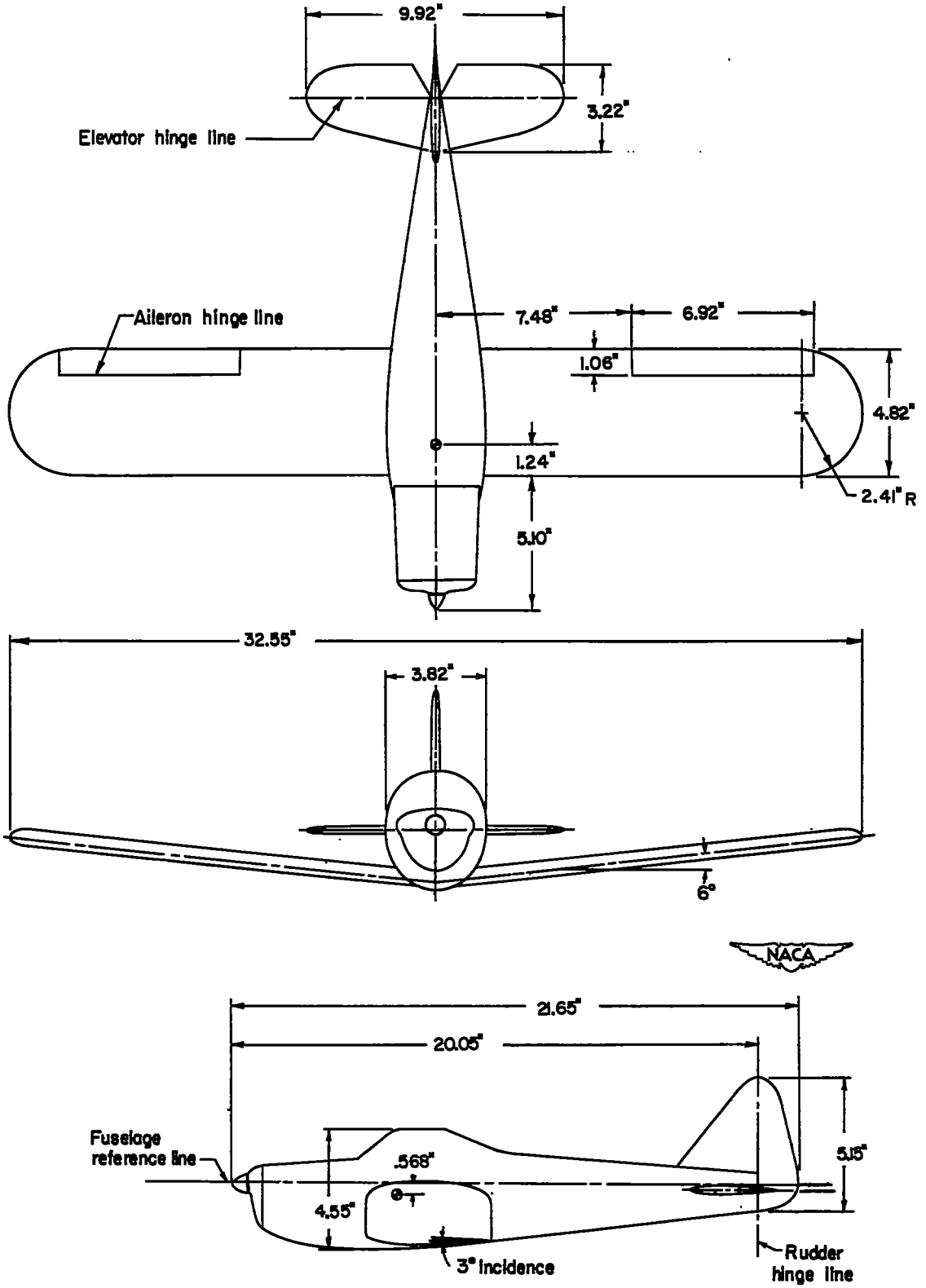

Figure 2.- Three-view drawing of model tested.

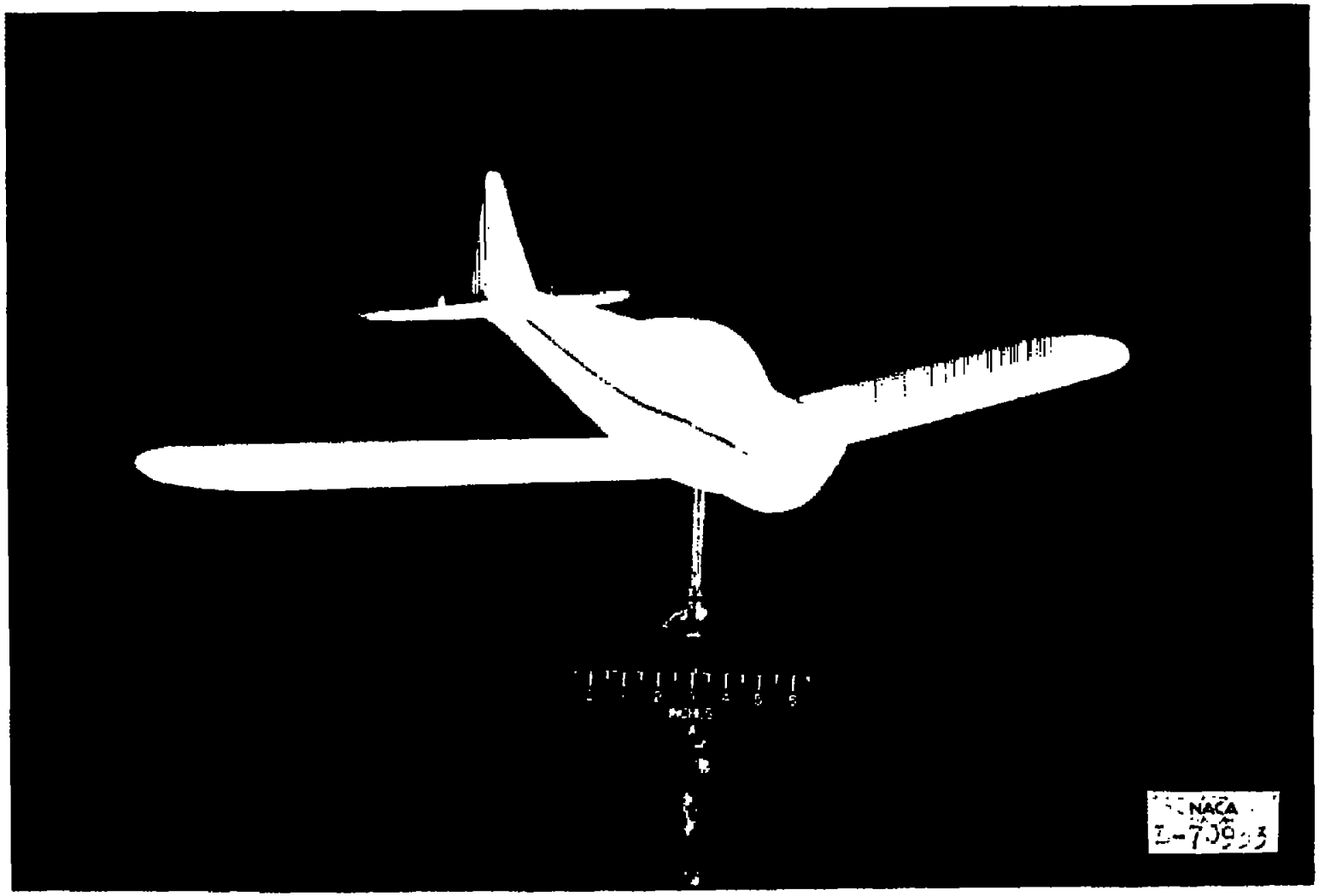

Figure 3.- Photograph of model tested.

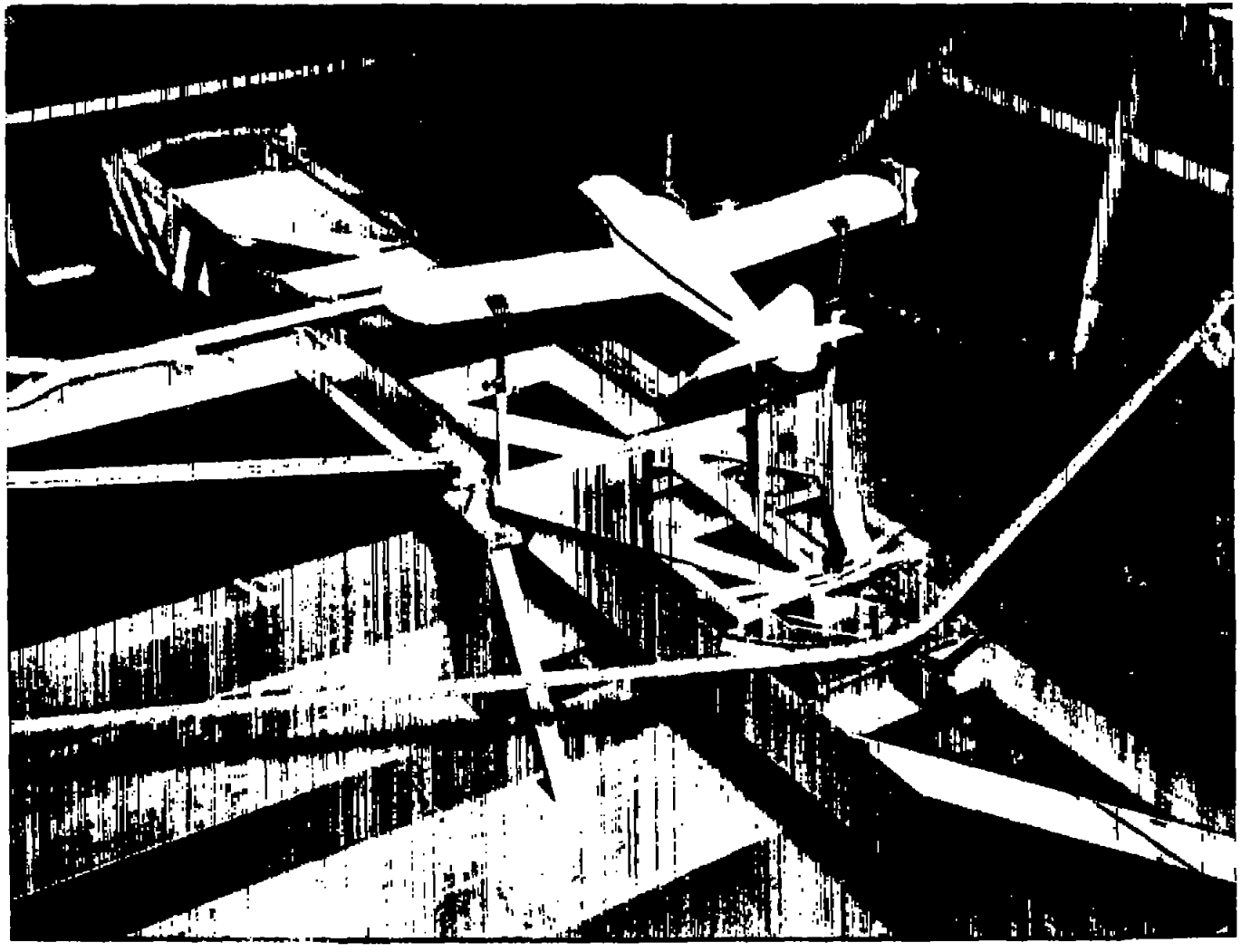

NACA L-76236.1

Figure 4.- Photograph of launching apparatus.

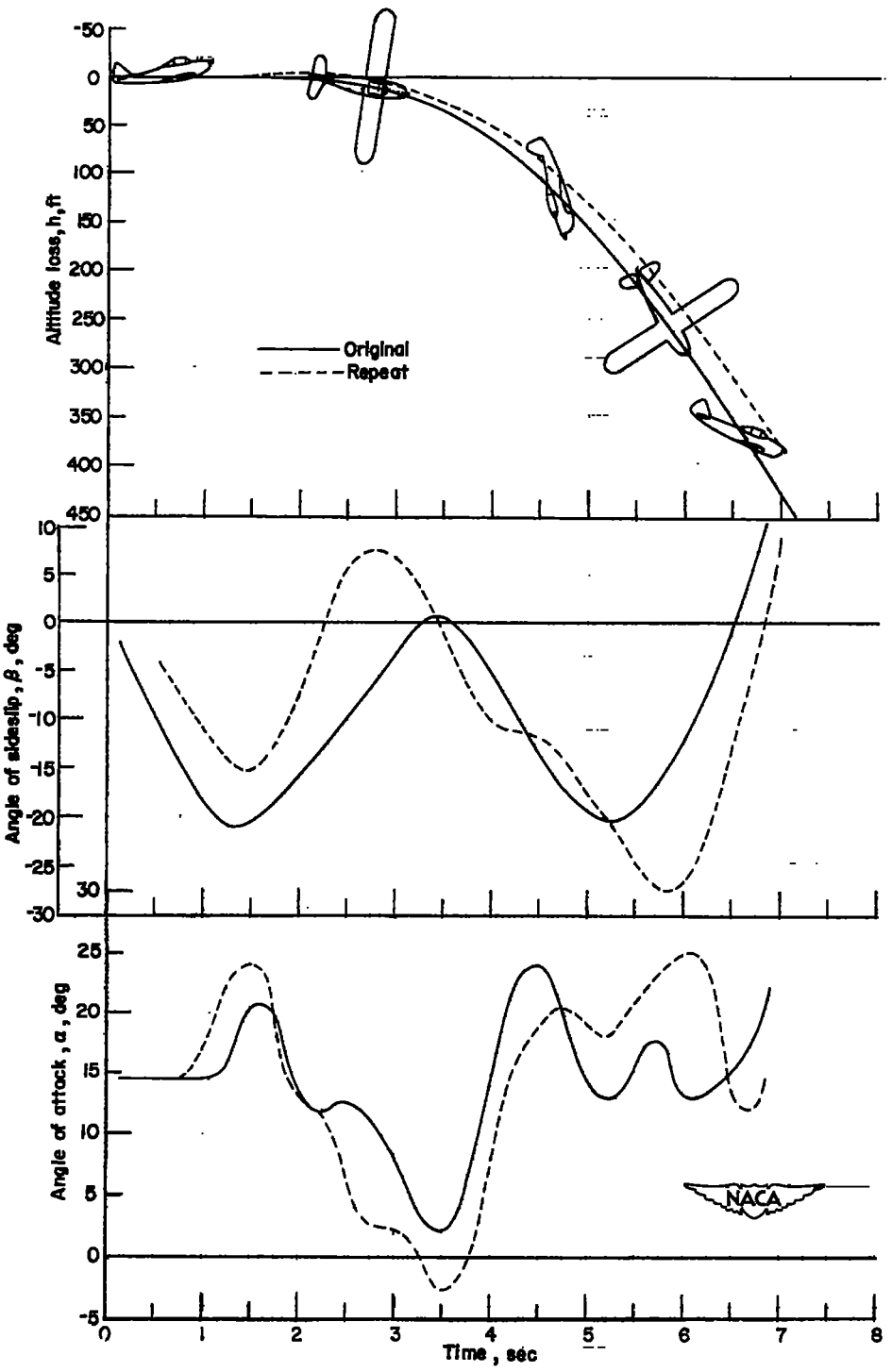

(a) Angle of attack, angle of sideslip, and altitude loss.

Figure 5.- Time histories of some components of model motion for the original and repeat right roll-offs.

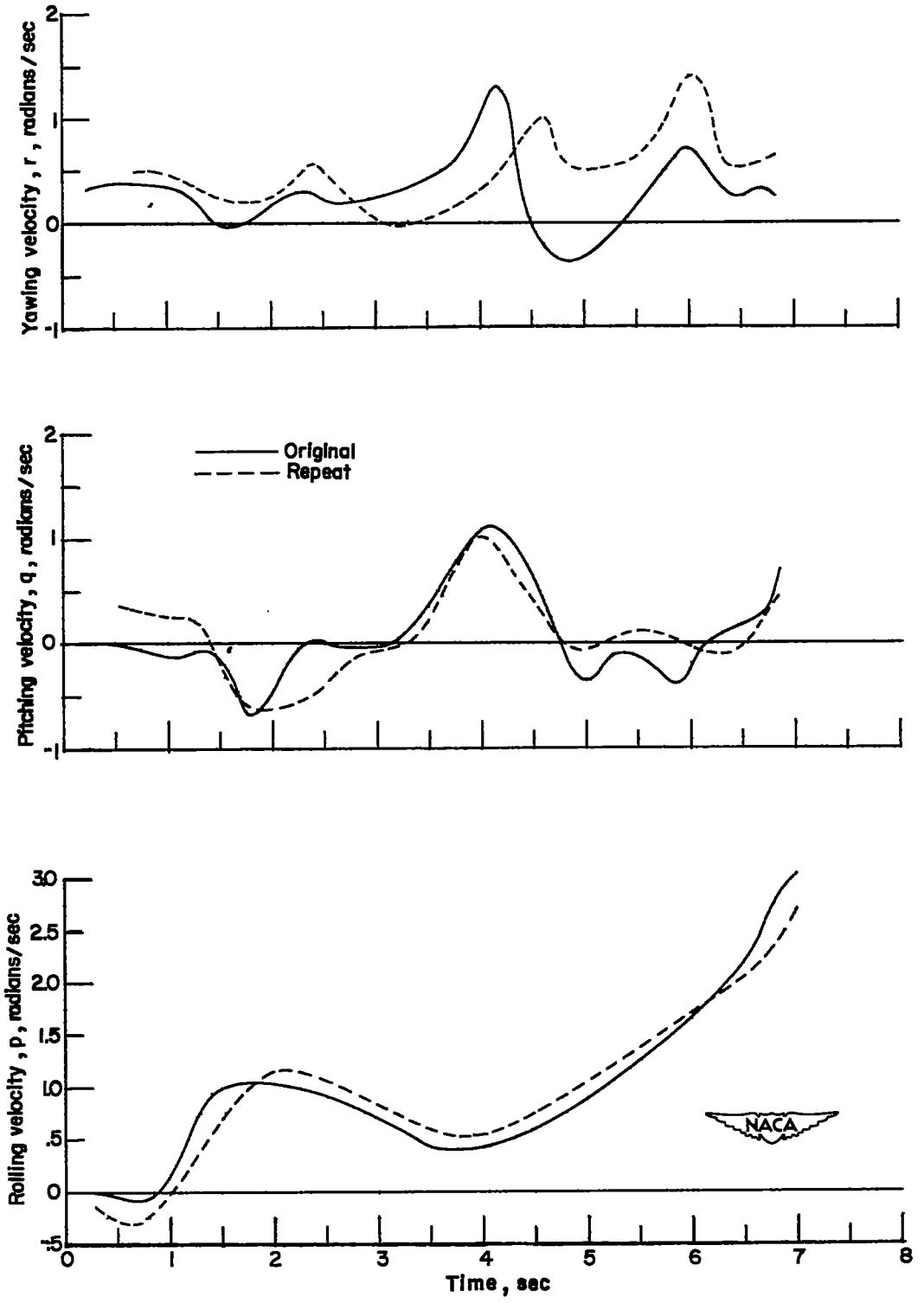

(b) Rolling, pitching, and yawing velocities.

Figure 5.- Concluded.

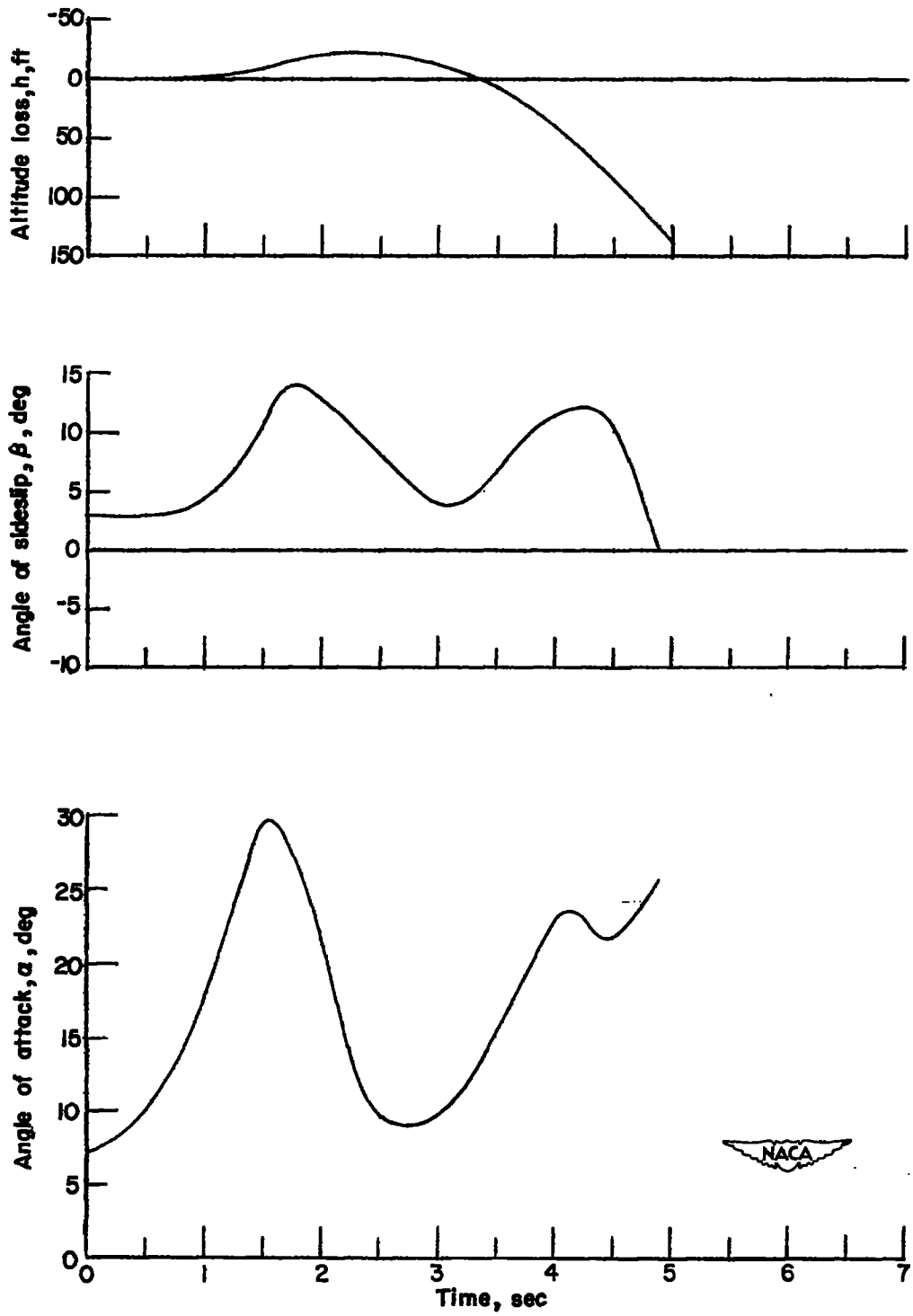

(a) Angle of attack, angle of sideslip, and altitude loss.

Figure 6.- Time histories of some components of model motion for the symmetry-check left roll-off.

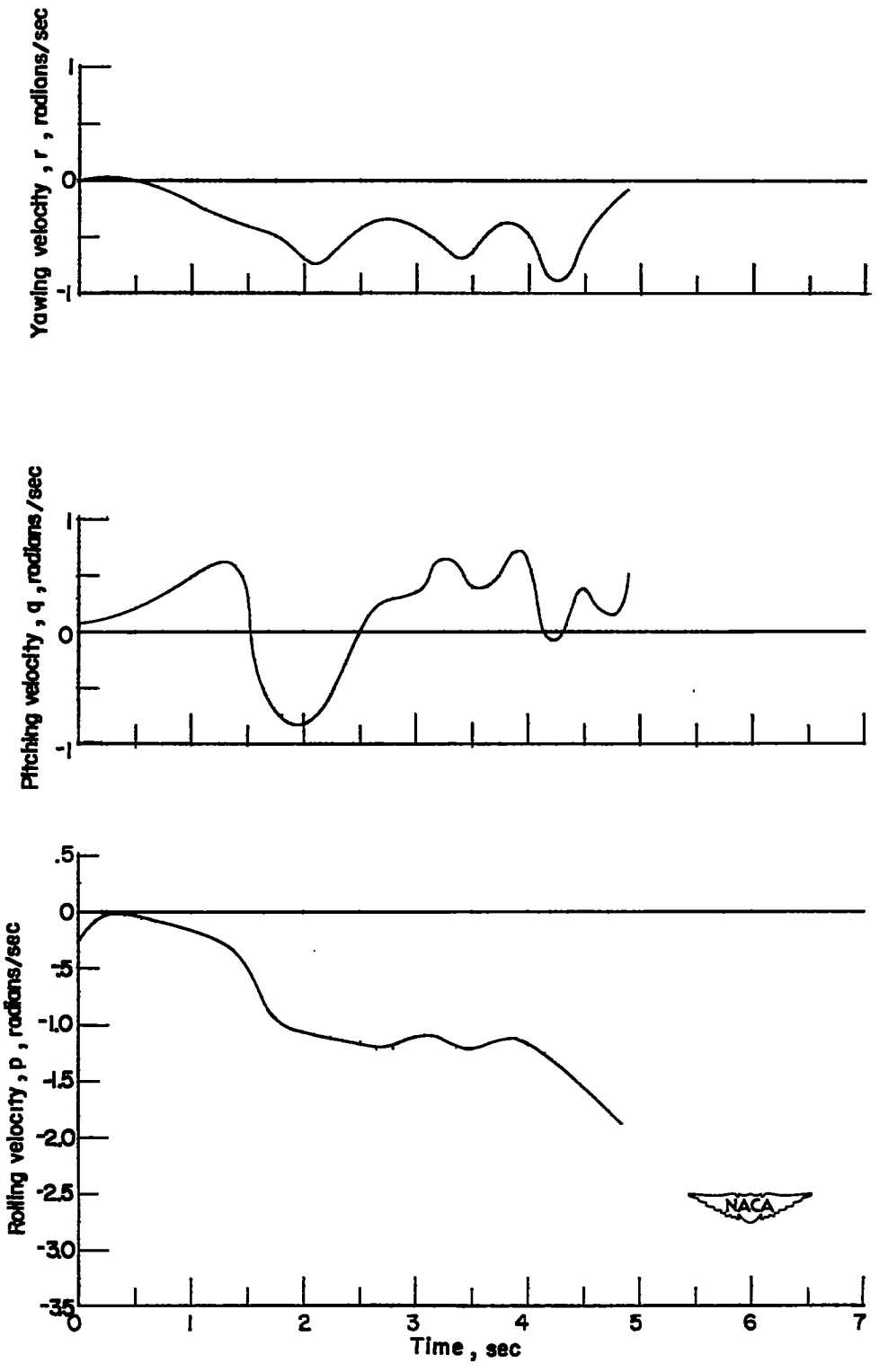

(b) Rolling, pitching, and yawing velocities.

Figure 6.- Concluded.

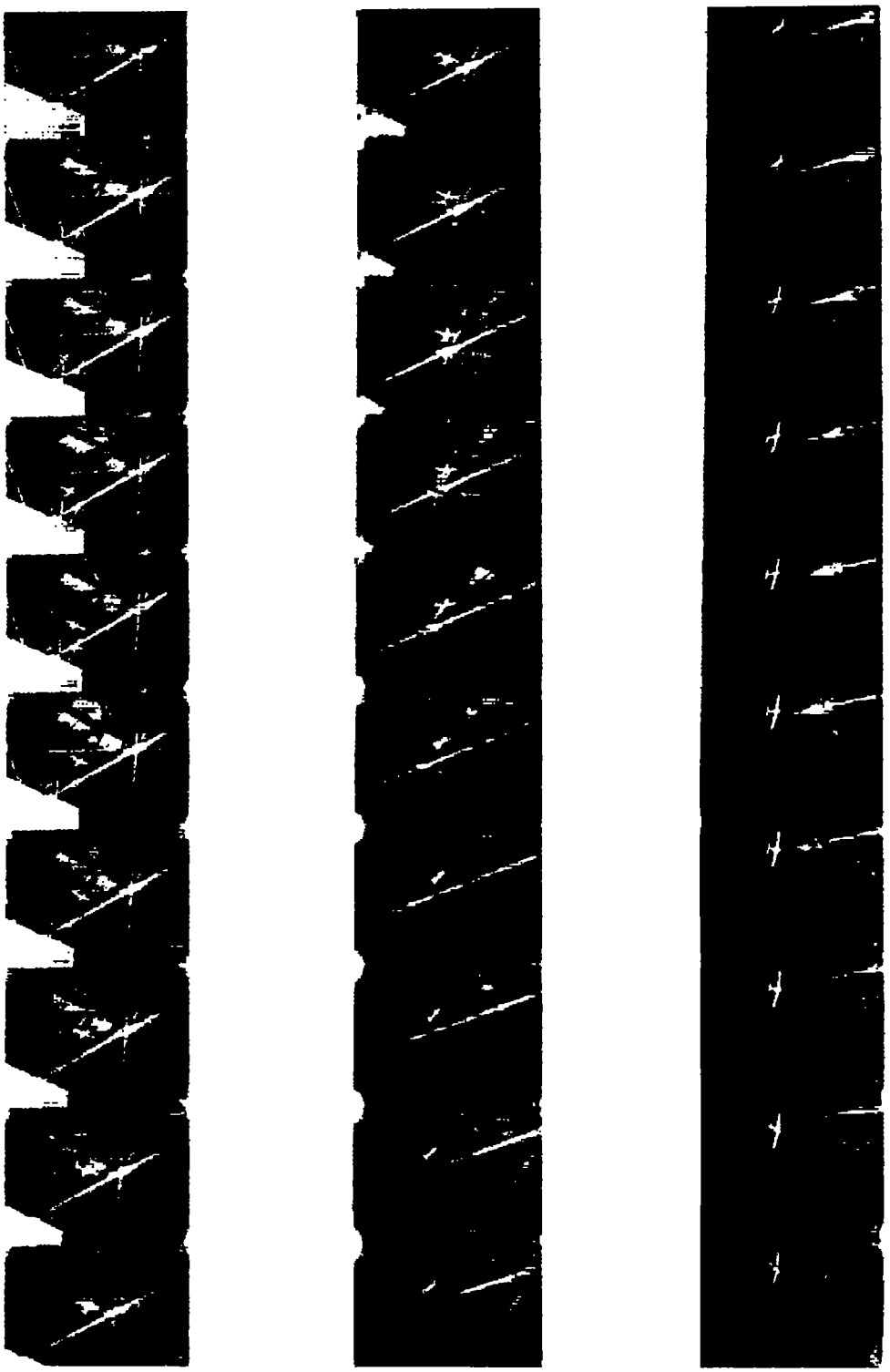

NACA
L-77935

Figure 7.- Panoramic view of the model motion in a right roll-off.

Figure 7.- Concluded. NACA L-77936

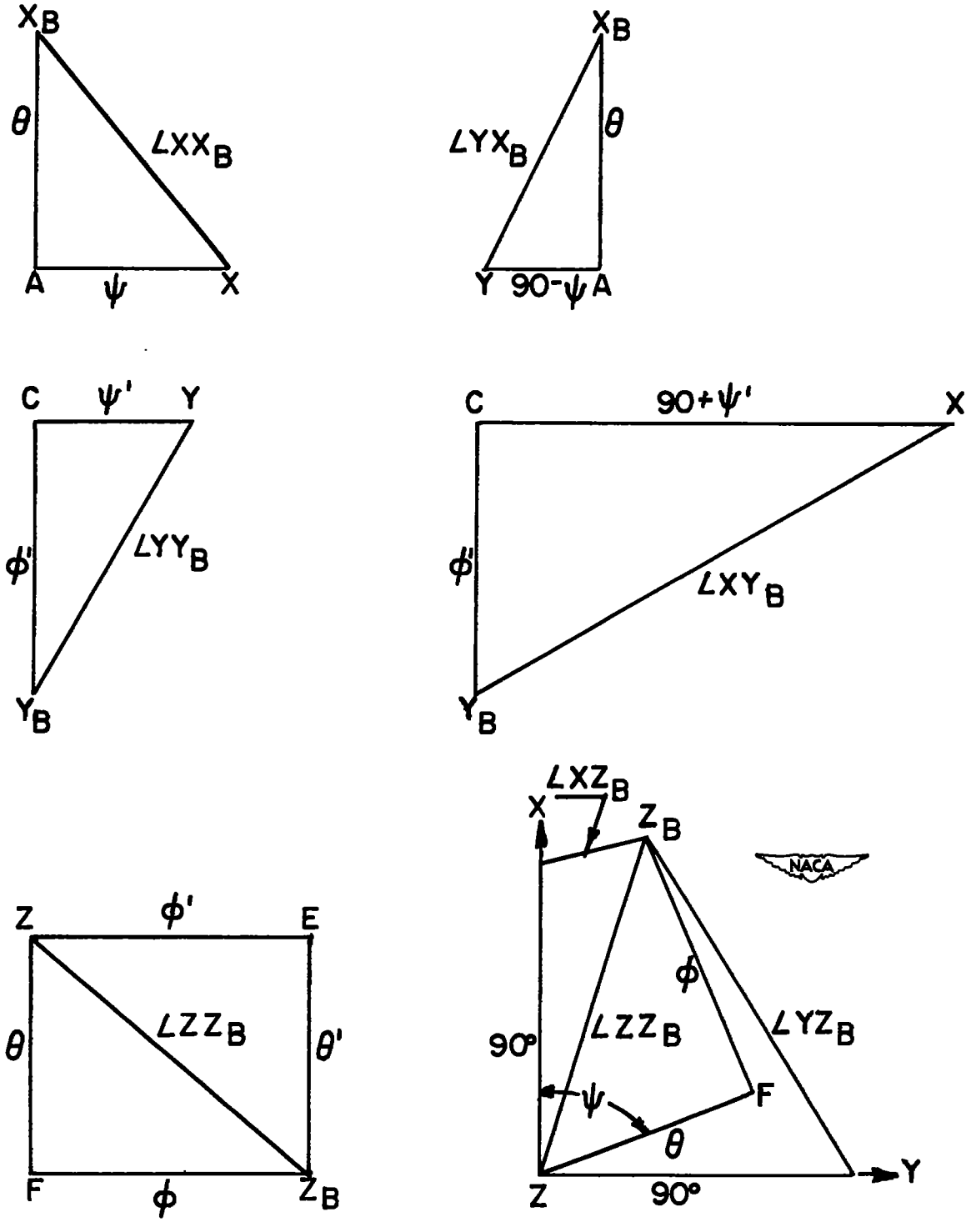

Figure 8.- Diagram of spherical triangles used in the analysis of data.

NACA-Langley - 4-10-53 - 325